Journal of Applied Biomedicine 14 (2016) 321–330

Contents lists available at ScienceDirect

Journal of Applied Biomedicine

journal homepage: www.elsevier.com/locate/jab

Original Research Article

Solid-state NMR study of discrete environments of bone mineral nanoparticles using phosphorus-31 relaxation

Agnieszka Kaflak[a,*], Dariusz Chmielewski[b], Waclaw Kolodziejski[a]

[a] Medical University of Warsaw, Department of Inorganic and Analytical Chemistry, Banacha 1, Warsaw, Poland
[b] Department of Orthopaedic Surgery and Traumatology, HOSPITEN Lanzarote, Spain

ARTICLE INFO

Article history:
Received 26 January 2016
Received in revised form 29 June 2016
Accepted 14 July 2016
Available online 26 August 2016

Keywords:
Apatite
Bone
Nanomaterial
Osteoarthritis
Osteoporosis
Nuclear magnetic resonance

ABSTRACT

Bone mineral nanoparticles, residing between collagenous fibres, contain a crystalline apatite core (CAC) covered by an amorphous hydrated surface layer (AHSL). The main objectives of this work were to characterize the nanoparticles of human bone mineral and their discrete CAC and AHSL regions and relate this information to bone diseases. This pilot study involved 18 postmenopausal women suffering from osteoarthritis together with osteoporosis or osteopenia. Trabecular tissue specimens were acquired from the femoral intertrochanteric region during total hip arthroplasty. The specimens of whole bone were examined by ^{31}P solid-state NMR (ssNMR) to measure the concentration ratio of phosphorus in the AHSL and CAC locations, together with their ^{31}P linewidths and spin-lattice relaxation times. It was found that the AHSL region of the studied specimens contained 13–24% apatite phosphorus. The magnitude, hydration and structural order of AHSL and CAC were dependent on the progress of the pertinent diseases. Thus, the ^{31}P ssNMR spectroscopy can be used *ex vivo* to selectively analyse the discrete nanoapatite environments in whole bone specimens and possibly assist in postoperative medical diagnostics.

Introduction

Bone may be considered an interpenetrating biological composite of mineral and collagen constituents (Fratzl et al., 2004; Fantner et al., 2006; Reznikov et al., 2014; Stock, 2015). Another crucial component is water, which is ubiquitous in the bone tissue and exerts a considerable effect on its biological and mechanical properties (Timmins and Wall, 1977; Cazalbou et al., 2004; Wehrli and Fernandez-Seara, 2005; Wilson et al., 2005; Wilson et al., 2006; Nyman et al., 2008; Techawiboonwong et al., 2008; Rey et al., 2009; Rai and Sinha, 2011; Rai et al., 2013; Wang et al., 2013; Pasteris et al., 2014; Samuel et al., 2014; Duer, 2015; Granke et al., 2015; Rai et al., 2015). The bone mineral structure can be studied at the nanosize level (Kaflak-Hachulska et al., 2003; Kolodziejski, 2005; Kaflak and Kolodziejski, 2007, 2008) and it shows differences in healthy and diseased bone tissue (Boskey and Coleman, 2010; Boskey, 2013; Bala and Seeman, 2015). In the present work specimens from postmenopausal women suffering from osteoarthritis (OA) and from osteoporosis (OPS) or osteopenia (OPA) are examined using solid-state NMR (ssNMR). Special attention has been given to the characterization of specific mineral compartments.

Bone mineral consists of apatite nanoparticles (platelets 8–40 nm long, 5–25 nm wide and 1-1.5 nm thick (Boskey and Coleman, 2010)), which have a crystalline apatite core (CAC) and an amorphous hydrated surface layer (AHSL) (Cazalbou et al., 2004; Wilson et al., 2005; Jäger et al., 2006; Wilson et al., 2006; Kaflak and Kolodziejski, 2008; Rey et al., 2009; Sakhno et al., 2010; Gaidash et al., 2011). Apatites are phosphate minerals, predominantly crystallizing in the hexagonal space group $P6_3/m$. The best

Abbreviations: OA, osteoarthritis; OPS, osteoporosis; OPA, osteopenia; ssNMR, solid-state NMR; CAC, crystalline apatite core; AHSL, amorphous hydrated surface layer; MAS, magic angle spinning; Min/matrix, the mineral-to-matrix ratio; CO_3/P, carbonate-to-phosphate ratio; XST, crystallinity; BMD, bone mineral density; PCA, principal component analysis; MSME, multi-slice multi-echo; *BV/TV*, bone volume to total volume ratio; BD, Bloch-decay (pulse-acquire NMR experiment); FWHM, full width at half maximum; DEXA, dual-energy X-ray absorptiometry; CrossLaps, β-CTX, C-terminal telopeptide of type-I collagen; Osteocalcin, bone γ-carboxyglutamic acid-containing protein; CV, coefficient of variation; *B/A*, concentration ratio of phosphorus in the AHSL and CPC locations; MSA, measure of sampling adequacy; CP, cross-polarization (polarization transfer in ssNMR); HPD, high-power decoupling.

* Corresponding author at: Medical University of Warsaw, Faculty of Pharmacy, Department of Inorganic and Analytical Chemistry, ul. Banacha 1, 02-097, Warszawa, Poland.
E-mail address: akaflak@wum.edu.pl (A. Kaflak).

http://dx.doi.org/10.1016/j.jab.2016.07.001
1214-021X/

known member of the apatite family, pure stoichiometric calcium hydroxyapatite $Ca_{10}(PO_4)_6(OH)_2$, is rare and difficult to synthesize. In fact, the bone apatite of CAC is non-stoichiometric, Ca^{2+} and OH^- deficient, and full of crystal defects and impurities (LeGeros, 1991; Cho et al., 2003). It contains carbonate ions CO_3^{2-} (4–6 wt %), mainly substituted for orthophosphate ions PO_4^{3-} (B-type substitution). CAC is covered by AHSL, which is 1-2 nm thick (Jäger et al., 2006; Bertinetti et al., 2007; Kaflak and Kolodziejski, 2008; Sakhno et al., 2010), contains 40-55% of apatite phosphorus (Jäger et al., 2006; Kaflak and Kolodziejski, 2008) and comprises ionic, non-apatitic environments regulating apatite reactivity and evolution (maturation, ion mobility and adsorption properties) (Cazalbou et al., 2004; Rey et al., 2009). Essentially, AHSL combines the mineral and the organic matrix (collagen) and provides bone with unique strength and resilience (Wilson et al., 2005; Wilson et al., 2006; Granke et al., 2015).

In recent years there has been a growing interest in the effects of hydration and dehydration on the properties of bone. It is surprising that latest ssNMR articles (Zhu et al., 2009; Xu et al., 2011; Mroue et al., 2012, 2014, 2015; McElderry et al., 2013; Gul-E-Noor et al., 2015) have not addressed the AHSL and CAC mineral compartments in the calcified tissues, although the importance of those environments is already well established (Combes et al., 2016). McElderry et al. (2013) performed joint ^{31}P ssNMR and Raman studies, but skipped the analysis of the ssNMR line components attributed to AHSL and CAC (Jäger et al., 2006; Kaflak and Kolodziejski, 2008) and of the 945-950 cm^{-1} Raman band assigned to amorphous phosphate or crystallographically disordered phase (Awonusi et al., 2007). Zhu et al. (2009) monitored only total water content in whole bone using ^1H ssNMR under MAS at 10 kHz. Other works from the Ramamoorthy group were mainly focused on the organic matrix (Xu et al., 2011, 2015; Mroue et al., 2012, 2014). Successfully, the ^1H ssNMR with ultra-fast MAS over 100 kHz (Mroue et al., 2015) and elaborate ^1H and ^2H relaxation studies of water in bone (Gul-E-Noor et al., 2015) were capable of resolving water in the apatite and collagen of the bone tissue. Such water associated with the apatite mineral and the collagenous matrix is called bound water, in contrast with the more mobile, liquid-like pore water of the haversian and the lacunocanalicular systems.

It is obvious that the bone tissue undergoes changes with aging and in diseases (Rosen et al., 1999; Rosen et al., 2013). However, the knowledge of those changes in the bone mineral is rather fragmentary and incomplete. Two recent reviews give a dependable summary of the latest results, mainly obtained using vibrational spectroscopic imaging (Boskey and Coleman, 2010; Boskey, 2013). In such studies conclusions are drawn from the area ratios of appropriate FT-IR or Raman bands. Therefore, the acquired chemical information has a relative sense and it is from the molecular level of bone. Thus, for animal models it is concluded that with increasing subject or tissue age, there is an increase in the mineral-to-matrix ratio (Min/matrix), carbonate-to-phosphate ratio (CO_3/P), relative OH^- content, Ca/P molar ratio and crystallinity (XST), while a decrease in the HPO_4^{2-} substitution is observed. In human bone, both cortical and cancellous, Min/matrix, CO_3/P and XST increase with age but the HPO_4^{2-} substitution decreases. In osteoporotic human cortical bone there is an increase in Min/matrix and XST, while CO_3/P remains unchanged. In osteoporotic human cancellous bone there is only an increase in XST, while Min/matrix and CO_3/P are not changed. The effect of OPS on the HPO_4^{2-} substitution in human bone mineral has not been yet determined.

The bound water in human cortical bone decreases with age, according to adequate group comparison (Granke et al., 2015) and bound water density correlates negatively with age (Seifert et al., 2014). However, the total cortical bone water (bound H_2O plus pore H_2O) increases 65% for postmenopausal women, compared to the premenopausal group (Techawiboonwong et al., 2008). It has been reported that the bound water content and the total water content both decreased in osteopenic-rat trabecular bone (Rai et al., 2013). Other work has demonstrated that amorphous phosphate material (ACP), which we suppose is located in AHSL, increased sharply in osteoporotic rat bone up to 36 vol. % (Gaidash et al., 2011). It seems that at least in the rat model, an increase in the AHSL magnitude caused by OPA or OPS is probably accompanied by some dehydration of this tissue compartment.

So far, no chemical information is available for the osteoarthritis effect on the mineral of human trabecular bone in the joints. The expected effect may be substantial, because the subchondral bone in OA has a higher bone mineral density (BMD) (Im and Kim, 2014). Maltsev et al. (2007) studied subchondral cortical bone from the joints of two horses with OA in comparison to reference material from three healthy animals. They did not find any differences between the mineral structure and composition of the specimens from diseased and healthy subjects. However, because of the small number of the studied cases, that conclusion ought to be verified. To the best of our knowledge, no work has reported the magnitude of AHSL and its water content in human or animal bone, neither in healthy nor in diseased tissues. In this work we show that this information can be obtained using classical ^{31}P relaxation measurements. Our working hypothesis is that NMR characteristics of the AHSL and CAC regions of bone apatite are dependent on OA and OPA/OPS bone diseases.

OA and OPS diseases in elderly people are huge health problems. In this project we have studied OA/OPS and OA/OPA specimens from whole bone taken during surgical operations of alloplastic reconstruction of the hip joints in postmenopausal women. The bone mineral has been specifically examined using ^{31}P ssNMR. The specimens have been investigated without any chemical pretreatment, so the organic matrix has not been removed or affected. Moreover, the samples have not been powdered, because the spectra were acquired without magic angle spinning (MAS). Thus, the studies were on intact bone without any interference to the tissue structure.

The ^{31}P NMR spectroscopy has successfully been applied to investigate tissue metabolites (Bartusik and Aebisher, 2015). In this work we analyse the bone mineral structure using saturation recovery measurements of the ^{31}P spin-lattice relaxation time T_1^P, coupled with appropriate ^{31}P ssNMR line deconvolutions and statistical principal component analysis (PCA). This original procedure allows us to observe the distribution of P-sites between the AHSL and CAC regions, probe hydration of those compartments and shed more light on patient classification. We suggest that it could be further implemented in the ^{31}P magnetic resonance medical diagnostics.

Materials and Methods

Preparation of specimens

The study was performed on 18 samples of human osseous tissue taken from Polish postmenopausal women suffering from OA together with OPS (14 patients) or OPA (four patients). Unfortunately, an adequate control group of postmenopausal women without bone diseases was not available for comparison purposes. Cylindrical core specimens of trabecular tissue, fitting 7 mm ssNMR rotors, were acquired from the femoral intertrochanteric region during total hip arthroplasty (details in Supporting Material). The samples were then lyophilized and sterilized (using γ irradiation of 3.5 KGy). Lyophilization does not affect the bound water from the bone mineral (Kaflak-Hachulska et al., 2003; Kaflak and Kolodziejski, 2007).

Ethics

The research was granted permission from the local research ethics committee of the Medical University of Warsaw. All procedures performed involving human participants were in accordance with the ethical standards of the institutional and/or national research committee and with the 1964 Helsinki declaration and its later amendments or comparable ethical standards. All patients were informed about the surgical procedure and their informed consent was obtained before surgery. No personal patient data were analysed or included in this work.

ssNMR and μMRI measurements

Solid-state ^{31}P NMR experiments were carried out to determine the molecular-level spectroscopic parameters characterizing bone mineral in the OA action site. The ssNMR spectra were acquired at 298 K using a Varian UNITY PLUS-200 spectrometer, working at 200 and 80 MHz resonance frequencies for ^{1}H and ^{31}P nuclei, respectively. The experiments were done with a Doty MAS probe using zirconia rotors (7 mm in diameter), but the samples were studied without rotation. We did not want to crush the samples for MAS, because such a procedure affects bone structure, in particular it disrupts the organic-mineral interface (Nikel et al., 2012). The cylindrical core samples (see Preparation of specimens) were only cut in lengths to fit the rotors. The ssNMR study was used to determine the spin-lattice relaxation time T_1^P. This is the time constant for the recovery of the longitudinal nuclear spin magnetization M_z of phosphorus-31, after resonance excitation, towards its thermal equilibrium value (M_z is parallel to the magnetic field of the spectrometer magnet). Since the relaxation time T_1^P of bone is about one hundred seconds (Kaflak and Kolodziejski, 2007), we used the saturation recovery technique. The saturation recovery is superior to inversion recovery because there is no need to use a long recycle delay of $5T_1^P$; this makes the relaxation measurement substantially faster. Each spectrum was recorded under high-power proton decoupling with 32 scans, π/2 pulses of 3.0 μs, recycle delays of three seconds and seven relaxation intervals from 10 to 640 s. The relaxation equations were fitted to experimental points with the KaleidaGraph program (version 3.5 for PC, Synergy Software 2000), which employs the nonlinear least-squares algorithm with the Levenberg-Marquardt gradient descent method of minimization of the error function.

Proton μMRI experiments were carried out to evaluate trabecular bone porosity in just the OA action site. They were done on the same specimens as in the ssNMR studies. The MRI images were acquired with a Bruker AVANCE 300 MHz WB spectrometer, using a microimaging probehead with a 15-mm coil, a maximum magnetic field gradient of 100 G/cm in the *x*,*y* and *z* directions, the Multi-Slice Multi-Echo (MSME) pulse sequence (T_R = 500 ms, T_E = 7 ms) and the proprietary Bruker microimaging software. With *FOV* of 10 × 10 mm^2 and the 256 × 256 data matrix the slice resolution was (39 μm)^2. For each sample, the bone volume fractions *BV/TV* (bone volume over total volume) were determined from 12 equidistant planar slices taken parallel to the bone cylinder axes; the mean value was then calculated.

Derivation of the ssNMR parameters

The ^{31}P ssNMR spectrum of bone contains one broad signal with a maximum at 3 ppm (Fig. 1a), which shows a two-component cross-polarization behaviour (Kolodziejski, 2005; Kaflak and Kolodziejski, 2008). This is because it contains a sharper main line from the CAC sitting on the top of a broader foundation line from the AHSL (Pajchel and Kolodziejski, 2013; Pajchel et al., 2013). Such an overlap of the CAC and AHSL lines also occurs for the Bloch-decay

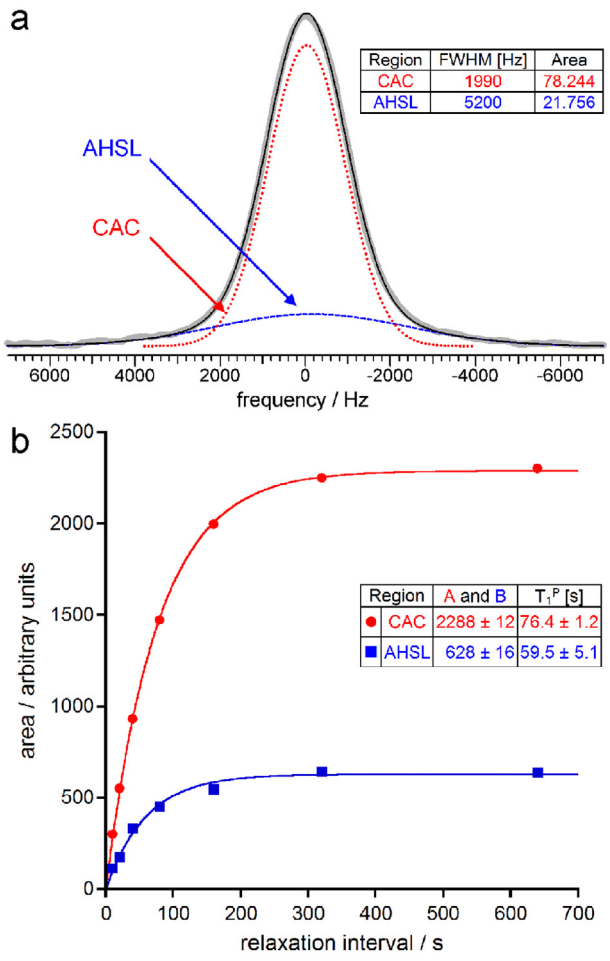

Fig. 1. Exemplary processing of the ^{31}P ssNMR spectra (F8): (a) signal deconvolution into the broad component from AHSL (dashed line) and the narrow one from CAC (dotted line); (b) fitting of Function 1 to the area points of the two component lines.

(BD) signals, recorded in our saturation recovery experiments. Thus, each complex ^{31}P ssNMR signal was decomposed into the CAC and AHSL components by line fitting (Fig. 1a), yielding linewidths (full widths at half maximum; that is, *FWHM* values) and component line areas.

Then, the relaxation function

$$I(\tau) = \Omega\,[1\text{-}\exp(-\tau/T_1^P)] \quad (1)$$

was separately fitted for CAC and AHSL to the component line areas $I(\tau)$, measured after various relaxation intervals τ (Fig. 1b). In this function, its amplitude Ω was equal either to the *A* or *B* areas of the fully relaxed CAC and AHSL components, respectively, and T_1^P was the spin-lattice relaxation time in the laboratory frame corresponding to the mineral region under consideration. Overall, the following five ssNMR parameters were measured: *B*/*A*, T_1^P-CAC, T_1^P-AHSL, *FWHM*-CAC and *FWHM*-AHSL.

Densitometry

Bone densitometry was done to determine the OPA or OPS disease stage of the skeleton. Dual-energy X-ray absorptiometric (DEXA) measurements were performed at the lumbar spine (L2–L4) before the surgical operation using a Lunar DXP-IQ densitometer. The apparatus was tuned and calibrated according to the manufacturer's advised protocol before each diagnostic session. The measured bone mineral density (BMD) was recalculated to the corresponding T-score value. According to the WHO, the T-score

values classify BMD as normal (−1 and above), osteopenic (between −1 and −2.5) and osteoporotic (−2.5 and below).

Markers of bone metabolism

The markers of bone metabolism were measured to assess the activity of osteoclast and osteoblast cells during bone remodelling. The biochemical tests were performed before the surgical operation. Venous blood samples were drawn in a fasting state in the morning. The serum was separated from the cells within three hours after collection of blood and stored at −40 °C before assays. Serum C-terminal telopeptide of Type-I collagen (CrossLaps, β-CTX) and bone γ-carboxyglutamic acid-containing protein (Osteocalcin) were measured by an Abbott analyser using the respective ELISA kits (Nordic Bioscence Diagnostics, Denmark). For CrossLaps, the intra- and interassay coefficients of variation (CVs) were both less than 8.1% and the detection limit was 0.02 ng × mL^{-1}. For Osteocalcin, the intra- and interassay CVs were 2.4% and 6.4%, respectively, and the detection limit was 0.5 ng × mL^{-1}.

Statistical analysis

Routine statistical analysis (correlation analysis and linear regression, group comparisons) was done using the Statistica 9.0 computer program (Stat Soft. Inc., 2009). The results of the correlation were evaluated by a p-value (probability level; significance of the relationship) and an R-value (correlation coefficient; the strength of the relationship). The correlation was considered significant for $p < 0.05$. Influential observations and outliers were identified using Cook's distance and the 4/N rule, where N is the number of cases. Principal component analysis (PCA) (Pett et al., 2003) was done using the statistical computer program SPSS 15.0 for Windows (SPSS Inc., 2006). All statistical analyses involving *BV/TV* were done for 15 cases only, because samples F2, F9 and F16 cracked after the ssNMR study and therefore were not examined using μMRI.

Results

General description of the results

In this study there are two main kinds of parameters to consider (Table 1). The first set is general, it includes Age and tissue-level measures of the skeletal system condition (T-score, CrossLaps, Osteocalcin). The second is local and comprises molecular-level ssNMR parameters of the bone mineral from the femoral-neck trabecular tissue (*B/A*, T_1^P-CAC, T_1^P-AHSL, *FWHM*-CAC and *FWHM*-AHSL). The first set of the parameters provides information on the bone pathological changes (OPS or OPA) and bone turnover, while the second allows one to monitor the mineral structure (morphology of nanoparticles and their chemical composition) just in the place where OA is operative (together with OPS or OPA, to some extent). The *BV/TV* parameter falls between the aforementioned groups. It is local, but provides information on the tissue level.

Regarding the general parameters (Table 1), Age and T-score are typical for postmenopausal women with OPA or OPS. CrossLaps and Osteocalcin are markers of bone resorption and bone formation, respectively. The reference intervals for postmenopausal women in ng × mL^{-1} are 0.09–1.05 and 8.0–40.9, respectively (Michelsen et al., 2013; Hannemann et al., 2013). The individual and mean values for our samples are within those reference ranges.

Concerning the local parameters (Table 1), first we comment on *B/A*. According to the former definitions, the *B/A* parameter denotes the concentration ratio of phosphorus in the AHSL and CPC locations. Thus, it is an indirect measure of relative magnitudes of those environments. In our specimens, *B/A* varies from 0.155 to 0.321. It follows that AHSL contains 13–24% of apatite phosphorus. Then, the relaxation times T_1^P are longer for CAC than for AHSL, by about 13% if mean values are compared. The NMR lines of CAC are approximately 2.5 times narrower than those of AHSL.

Finally, we note that in literature there are *BV/TV* values for subchondral trabecular bone in postmenopausal women with OA and with OPS (Zhang et al., 2009): 21.55 ± 3.41% and 16.64 ± 2.26%, respectively. Our mean value of 29 ± 13% (Table 1) is indicative of advanced osteoarthritis.

Correlation analysis

The correlation analysis was carried out to check whether the specimen parameters have a linear relationship with each other. Such a relationship may help infer associations among those variables.

It is intriguing that there is no significant correlation between the general and ssNMR parameters. Only T-score shows a high negative correlation with *BV/TV* ($0.5 < |R| < 0.7$; cf. Fig. 2 and Table 2).

Most interestingly, there are significant correlations between the local parameters from ssNMR (Fig. 3, Table 2). Apart from that

Table 1
Characteristics of the studied population (n = 18). Four women had osteopenia (T-score between −1 and −2.5) and the rest suffered from osteoporosis (T-score < −2.5).

Variable	Mean ± SD	Range
General characteristics		
Age (years)	64.4 ± 6.7	50–77
BMD L2–L4 (g × cm^{-2})[a]	0.876 ± 0.051	0.832–0.990
T-score	−2.73 ± 0.48	from −1.6 to −3.3
CrossLaps (ng × mL^{-1})	0.187 ± 0.144	0.060–0.519
Osteocalcin (ng × mL^{-1})	30.7 ± 7.2	17.5–39.2
μMRI characteristics		
BV/TV (%)[b]	29 ± 13	11–53
Solid-state NMR characteristics		
B/A	0.256 ± 0.052	0.155–0.321
T_1^P-CAC (s)	77.0 ± 6.3	69.0–90.1
T_1^P-AHSL (s)	67 ± 14	33.4–89.5
FWHM-CAC (Hz)	2001 ± 21	1970–2048
FWHM-AHSL (Hz)	5580 ± 440	4977–6562

[a] Determined *in vivo* using DEXA.
[b] Determined for 15 cases.

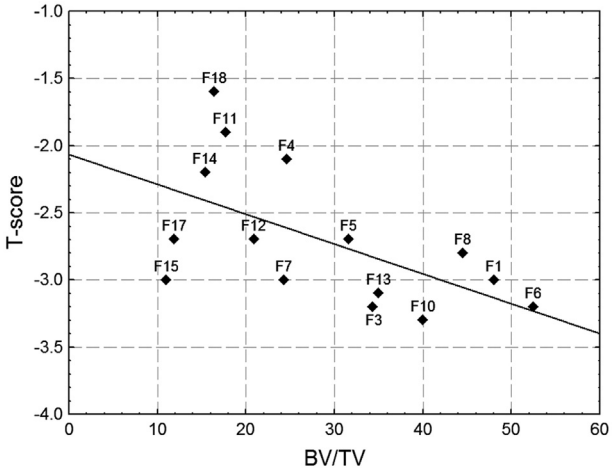

Fig. 2. The relationship between T-score and *BV/TV*. Statistical details are given in Table 2.

Table 2
Correlations observed between the specimen parameters. T_1^P and *FWHM* values are given in s and Hz, respectively and *BV/TV* in %.

$y = ax + b$						
N	*y*	*x*	R	p	*a*	*b*
15	T-score	*BV/TV*	−0.575	0.025	−0.0221	−2.07
18	T_1^P-CAC	*B/A*	0.656	0.0031	79	56.9
18	T_1^P-AHSL	*B/A*	0.754	0.00030	200	16
18	*FWHM*-CAC	*B/A*	−0.827	0.000023	−337	2087
18	*FWHM*-AHSL	*B/A*	−0.848	0.000009	−7100	7400
18	T_1^P-CAC	T_1^P-AHSL	0.706	0.0011	55.5	0.321
18	*FWHM*-CAC	*FWHM*-AHSL	0.739	0.00046	0.0357	1801
18	ΔT_1^{Pa}	*B/A*	−0.607	0.0076	−121	40.6

[a] The difference between the T_1^P values of CAC and AHSL.

between T_1^P-CAC and *B/A*, they are very high ($0.7 < |R| < 0.9$). For both AHSL and CPC, there are positive correlations of T_1^P and negative correlations of *FWHM* with *B/A*.

All the observed correlations are robust in the sense that the correlation coefficients and regression parameters are hardly affected by removing outlying cases (see Supporting Material).

Principal component analysis

The ssNMR parameters have been subjected to PCA to reduce the number of the variables. The detailed PCA report is given in Supporting Material and selected results are shown in Table 3. According to the Kaiser Rule (one eigenvalue found over 1), Variance Extracted Criterion (over 70% found for *PC1*) and Cattell's Scree Test (visual decision), only one principal component (*PC1*) is sufficient to represent our ssNMR variables (Table 3). This PCA solution has been treated with special caution because of the limited number of cases (18). Therefore, after examining the pertinent literature, we decided to follow Zhao's recommendations for such PCA problems (Zhao, 2009): overall KMO over 0.60, communalities of all variables over 0.60, the mean value of all communalities over 0.70, the Kaiser's strategy (dropping all components with eigenvalues under 1.0) and the Scree plot to determine the number of factors, absolute values of all loadings over 0.60, retention of factors with three and more variables.

Finally, we have one component with five variables representing the case-to-variable ratio of 3.6 (18/5) and the variable-to-component ratio of five. The overall KMO measure of sampling adequacy (MSA) is 0.662 with the diagonal elements of the Anti-Image Correlation Matrix (the MSAs for the individual variables) in the 0.579–0.890 range. The minimum, maximum and mean values of the communalities are 0.58, 0.96 and 0.71 (SD = 0.15), respectively. The absolute values of *PC1* loadings are in the 0.760–0.977 range. There are no cross-loadings, because only one component has been extracted. Thus, in principle, Zhao's recommendations have been fulfilled.

Furthermore, we have verified our PCA solution using the leave-one-out procedure (see Supporting Material). It has been found that for each of the 18 cases the *PC1* variance under the leave-one-out procedure is low and has no influence on the clustering of those cases. The standardized Cronbach's alpha was 0.881, which is in the

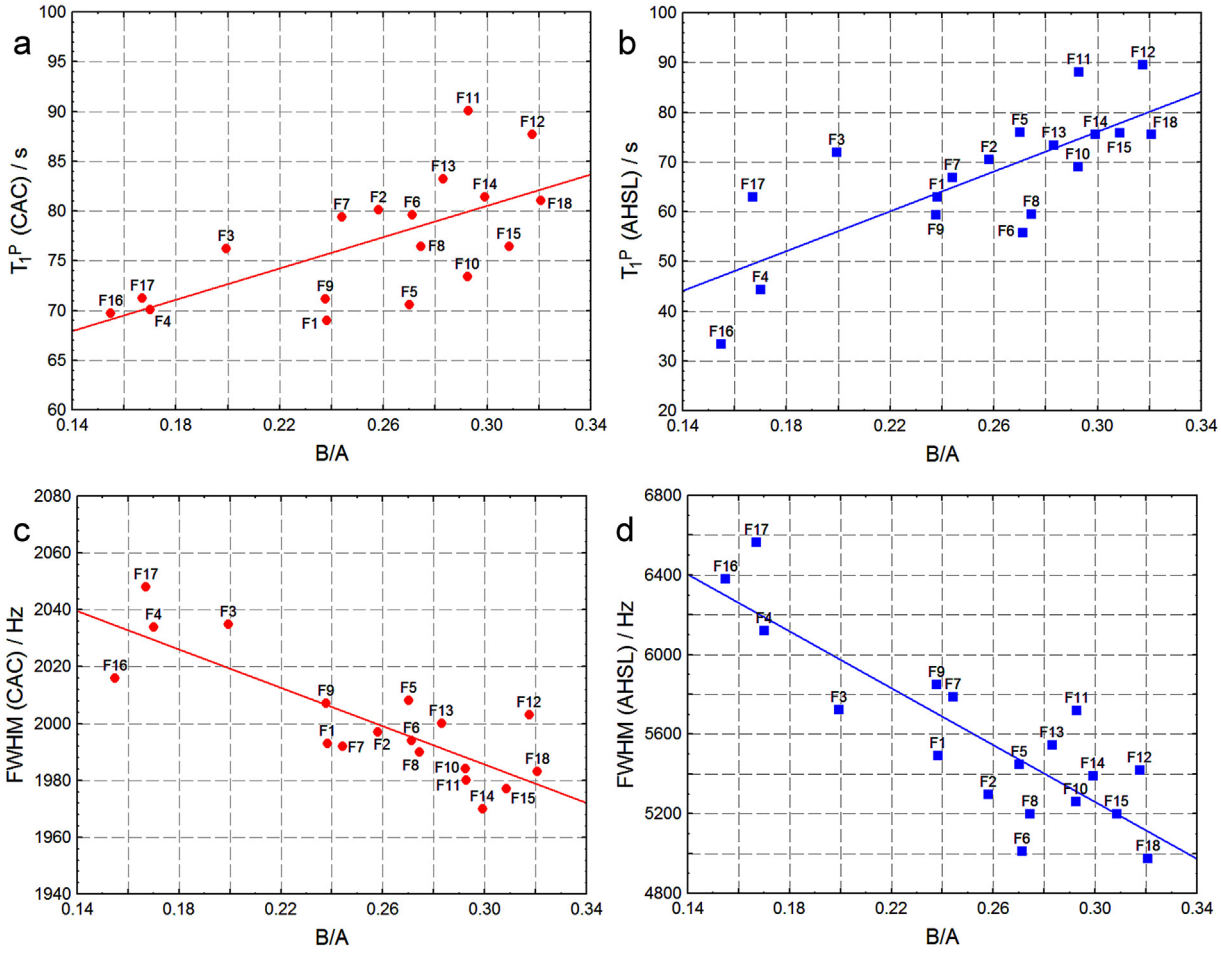

Fig. 3. Linear regression graphs of various ssNMR parameters against B/A: (a) T_1^P of CAC; (b) T_1^P of AHSL; (c) *FWHM* of CAC; (d) *FWHM* of AHSL. Statistical details are given in Table 2.

Table 3
Selected results of the principal component analysis of the ssNMR parameters.

Extraction of the principal components		
PC	Eigenvalue	Cumulative variance (%)
1	3.551	71.0
2	0.843	87.9
3	0.348	94.8
4	0.218	99.2
5	0.040	100.0
PCA characteristics of the variables		
Variable	Communalities from *PC1*	Factor loadings for *PC1*
B/A	0.955	0.977
T_1^P-CAC (s)	0.578	0.760
T_1^P-AHSL (s)	0.628	0.793
FWHM-CAC (Hz)	0.696	−0.834
FWHM-AHSL (Hz)	0.694	−0.833

acceptable 0.7–0.9 range (computed using the FACTOR program of Lorenzo-Seva U and Ferrando PJ, Release Version 9.2, Rovira i Virgili University, Tarragona, Spain, 2013).

Selection and characterization of patient groups

The next step in the analysis was to apply the new *PC1* variable to a comprehensive examination of the studied cases. The cluster analysis involving two local parameters, *PC1* and *BV/TV*, selects three groups of patients (Fig. 4a). The same groups are indicated when the T-score is included in the cluster analysis (not shown). The groups G1 (five cases), G2 (eight or 10 cases) and G3 (two or three cases) are clearly seen, when *BV/TV* (Fig. 4b) and T-score (Fig. 4c) are plotted against *PC1*. The median values of *PC1* for those groups in Fig. 4c are 1.11, 0.13 and −1.78, respectively.

Then, the differences in various parameters between the selected groups have been analysed using the non-parametric Kruskal-Wallis test (Fig. 5). The statistically significant differences were found in *PC1* between all three groups and in *BV/TV* and T-score between G1 and G2. G1 has a lower *BV/TV* and higher T-score, while G2 has a higher *BV/TV* and lower T-score. The G3 group is rather peculiar, because it has the biggest levels of CrossLaps and Osteocalcin, indicating a high bone turnover.

Discussion

Hypothesis and findings to discuss

Our leading hypothesis was that the NMR characteristics of the AHSL and CAC regions of bone apatite (Table 1) are dependent on the bone diseases OA, OPA and OPS. To prove it, we have determined general, macroscopic parameters of the skeletal system and the local, molecular-level ssNMR parameters of the bone mineral. Then, the parameters were subjected to statistical analysis to find correlations between them and to reduce the data set using PCA. The PCA procedure allowed us to divide patients into three groups. In the following discussion, we want first to translate the accumulated spectroscopic knowledge into chemical information on the AHSL and CAC environments of bone nanoapatite. Next, the patient groups have to be assigned to bone diseases. Then, the impact of the specific bone diseases on AHSL and CAC has to be determined. Finally, we wish to discuss the relationship between OA and OPS and comment on the possible applications of our methodology.

Relative magnitudes of the AHSL and CAC regions

First of all, it is worthwhile to comment on the bone apatite structure and hydration. From the *B/A* values (Table 1) one can

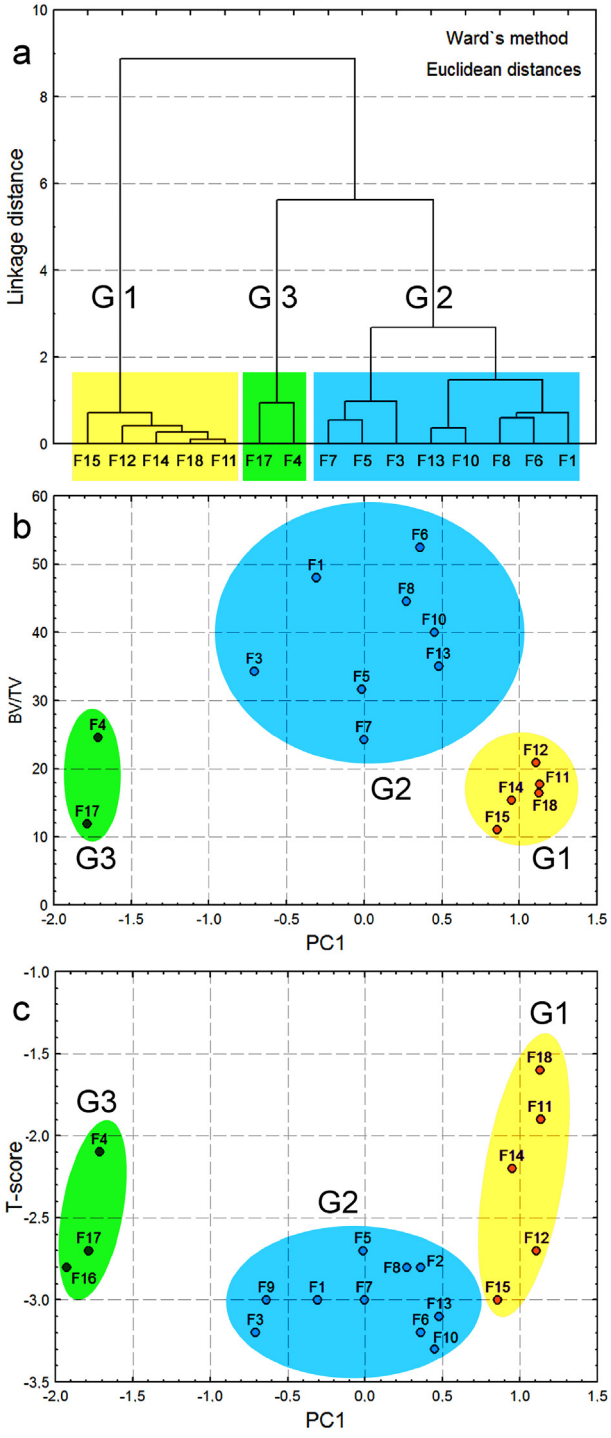

Fig. 4. Various plots pertinent to the group selection: (a) results of the cluster analysis, involving the principal component *PC1*, representing the ssNMR parameters, and *BV/TV* from μMRI; (b) the plot of *BV/TV* against *PC1*; (c) the plot of T-score against *PC1*. The G2 and G3 populations in the graphs B and C are different, because the *BV/TV* values for F2, F9 and F16 have not been determined.

easily calculate that the bone apatite particles of the studied specimens contain up to 24% of their phosphorus within AHSL. This BD estimation is probably more accurate than the previous one (40–55%) based on cross-polarization (CP) from protons to phosphorus-31 (Jäger et al., 2006; Kaflak and Kolodziejski, 2008). The CP estimation of the AHSL magnitude gives larger values because CP emphasizes the proton-rich apatite surface over its proton-deficient interior (Wu et al., 2002).

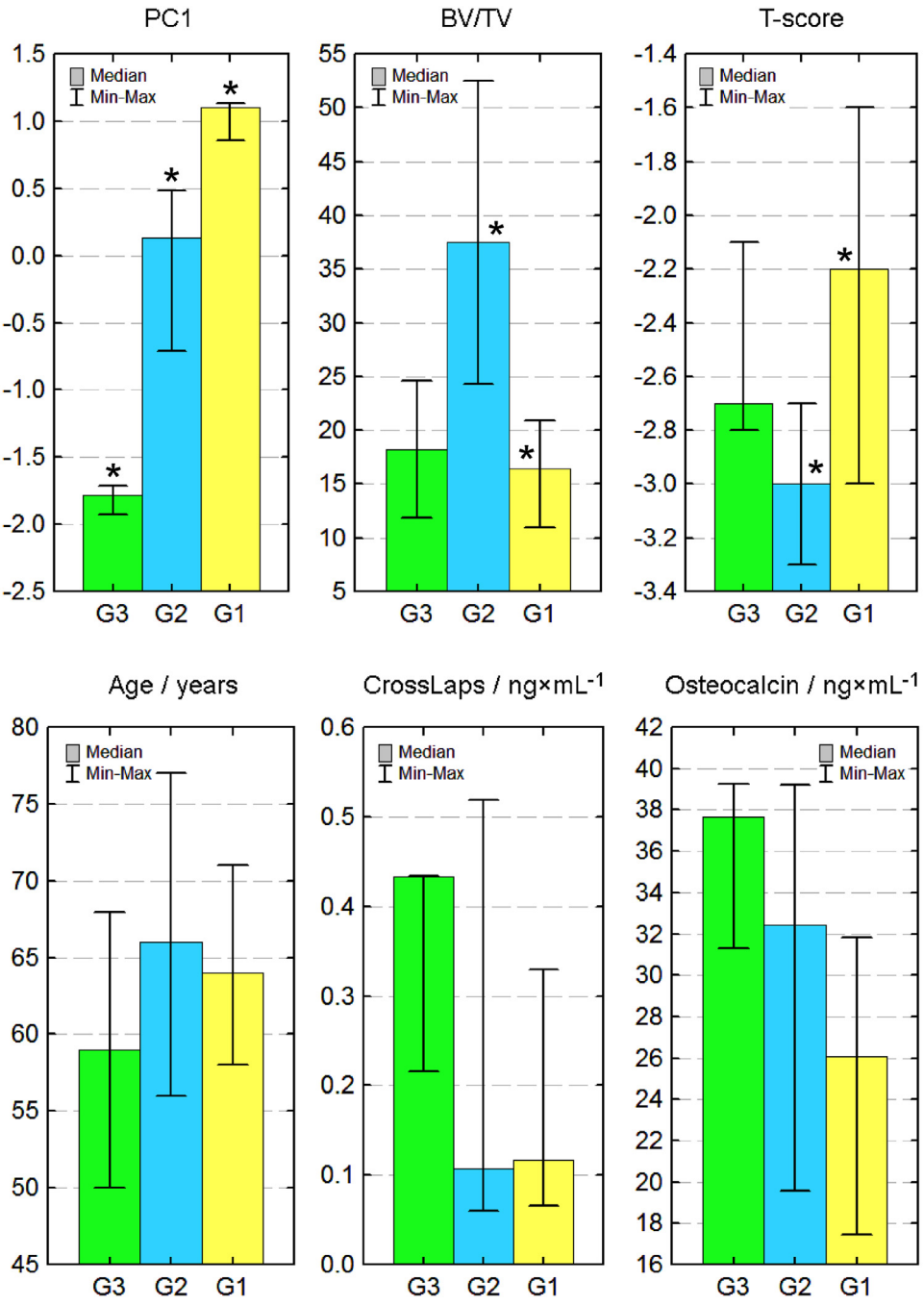

Fig. 5. Column and whisker plots of various parameters of the selected groups. Asterisks denote statistically significant differences in parameters between the marked groups (Kruskal-Wallis ANOVA).

Hydration and structural order of the AHSL and CAC regions

Our AHSL estimation indicates that CAC is covered by a quite thick AHSL. It turns out that AHSL must have an important influence on the bone apatite properties. This region has a lower T_1^P and larger *FWHM* (Table 1). Consider that T_1^P of the bone apatite decreases on hydration (Dawson et al., 1991; Kaflak and Kolodziejski, 2007) and that *FWHM* increases with structural disorder (Pajchel and Kolodziejski, 2013). It follows that AHSL is more hydrated and disordered than CAC. This statement is consistent with the knowledge that the former region is prone to water adsorption and is amorphous, while the latter is crystalline and thereby unable to accommodate abundant water (below 3 wt % of intracrystalline structural water in synthetic nanoapatite according to Pasteris et al., 2014).

Interdependence of the AHSL and CAC regions

Then, the correlations in Fig. 3 demonstrate that T_1^P and *FWHM* increase and decrease, respectively, with the increase of *B/A* (cf. also Table 2). This observation is valid for both CAC and AHSL. Thus, when AHSL grows, both AHSL and CPC become less hydrated and

more ordered. Such congruence of the two regions requires more explanation. It has been reported that AHSL affects CPC, in particular by supplying water molecules to the crystal channels (Pajchel and Kolodziejski, 2013). This interphase hydration phenomenon introduces structural disorder into the crystalline lattice of CAC. Therefore, it is comprehensible that the AHSL and CAC bone mineral regions influence each other and that their T_1^P and *FWHM* parameters may vary in concert. That is why there are correlations between T_1^P-CAC and T_1^P-AHSL, and between *FWHM*-CAC and *FWHM*-AHSL (Table 2). An NMR spectroscopist would suppose that it must be some inter-domain averaging of the T_1^P values of CAC and AHSL, caused by ^{31}P spin diffusion. Such averaging would have decreased the difference ΔT_1^P between the T_1^P values of CAC and AHSL with the relative decrease of AHSL (that is with the decrease of B/A). If it exists, such process is ineffective because the correlation between ΔT_1^P and B/A is the opposite to that expected for the relaxation averaging to be decisive (Table 2).

Features of the patient groups

Our study shows that the five ssNMR variables (*B/A*, T_1^P-CAC, T_1^P-AHSL, *FWHM*-CAC and *FWHM*-AHSL) can be represented by one principal component (*PC1*). This renders patient classification easier and more informative. Considering the *PC1* loadings for those variables (Table 3), AHSL grows (increase of *B/A*) with the increase of *PC1*, both CPC and AHSL become less hydrated (increase of T_1^P-CAC and T_1^P-AHSL) and more ordered (decrease of *FWHM*-CAC and *FWHM*-AHSL).

Two main groups of women have been discerned (Fig. 4): (G1) median *PC1* = 1.11, lower median *BV/TV* = 16.4, higher median T-score = −2.2; (G2) median *PC1* = 0.13, higher median *BV/TV* = 37.5, lower median T-score = −3.0. The differences in the *BV/TV* and T-score between those groups are significant (Fig. 5). The third group (G3) with median *PC1* of −1.78 is peculiar, because it is the smallest and has the highest bone turnover. The median *BV/TV* and T-score values of G3 are equal to 18.3 and −2.7, respectively. G2 includes only the OPS subjects, while the OPA subjects are spread between G1 and G3.

Interpretation of the patient groups

Contrary to common opinion, OA and OPS or OA and OPA can coexist in the same individual (Glowacki et al., 2003; Sun et al., 2008). Our patients were osteoarthritic (assessed by the radiological examination of the hip joint) and either osteoporotic or osteopenic (according to the lumbar spine T-score). For OA, an elevated BMD was found in the subchondral trabecular bone in the joints (Im and Kim, 2014). In our study a higher BMD in a specimen, that is, more advanced OA, can be assessed by its higher *BV/TV* value. Indeed, it has been found that *BV/TV* is significantly higher in OA than in OPS (Zhang et al., 2009). For OPS, a lower T-score (i.e., with the bigger absolute value) informs one about more advanced disease.

Therefore, in view of the *BV/TV* and T-score parameters, the women of G1 had less advanced OA and OPS than those in the G2 group. Considering the bone mineral particles, it can be concluded from *PC1* that G1 had larger AHSL than G2 and had less hydrated AHSL and CAC; however, those environments were more ordered in the chemical structural sense. To be more specific, for the purpose of this work, the more ordered environment is thought to have a more uniform distribution of P-containing species (ions, molecules) and therefore a sharper ^{31}P ssNMR line.

Relationship between osteoarthritis and osteoporosis

As has already been demonstrated, for all the studied specimens there is a negative correlation of T-score with *BV/TV* (Fig. 2, Table 2). According to the former discussion, this correlation can be interpreted as an increase of OA with an increase of OPS, treating OPA as an early stage of OPS. Moreover, in the former section we have mentioned an increase of OA together with OPS, when going from G1 to G2. All these findings go against the inverse relationship between OA and OPS postulated in the literature (Zhao, 2009) and understood as the exclusion or inhibition of the latter disease by the former. However, it must be admitted that in the area of the OA affected joint, this disease is far more influential than OPS and acts against OPS with success, elevating the BMD of the involved trabecular bone. The bone mineral affected by OA undergoes significant alteration, which can be deduced from the *PC1* values of G1 and G2: AHSL decreases comparing to CAC, both environments acquire more water and become less ordered. For CAC, increased disorder corresponds to a decrease in crystallinity.

It is unclear why OA is associated with increased BMD of the trabecular bone in the vicinity of the diseased joint (Im and Kim, 2014). Among various reasons, abnormal bone metabolism, composition and ultrastructure are usually debated. Considering our results, we can only address very few aspects. Thus, it has been found that postmenopausal women with OA had the serum Osteocalcin level increased by about 20% compared to those with OPS (Jiang et al., 2008). We have observed similar (although uncertain) excess of Osteocalcin in G2 over G1 (Fig. 5), which is in the patient groups with more and less advanced stages of both bone diseases, respectively. As the CrossLaps levels for G2 and G1 were almost the same (Fig. 5), it might be the increased bone formation in G2 around the OA affected joint. However, even if this hypothesis is true, the elevated BMD in G2 due to OA (Fig. 5; see the significant difference in *BV/TV* between G2 and G1) is associated with a pathological bone growth. We have already pointed out that OA modifies the bone mineral: AHSL decreases compared to CAC, both environments acquire more water and become less ordered. Such mineral changes are consistent with the literature information that trabecular bone from human femoral heads of OA subjects was more hydrated compared to a healthy group (Li and Aspden, 1997).

Claims, limitations and prospects

We have proved that the AHSL and CAC environments of bone nanoapatite can be monitored *ex vivo* in whole bone using ^{31}P ssNMR. In particular, the phosphorus content, hydration and structural order of those discrete mineral regions can be investigated. The mentioned characteristics are dependent on the bone diseases (OA, OPA and OPS), so their application in medical diagnostics is worth considering.

The study has some limitations. It was not possible to gather an appropriate healthy reference group. The studied group was limited to 18 cases. We had no access to MRI/MRS apparatus capable of acquiring ^{31}P images and spectra from selected body parts. Therefore, we could not extend our work to *in vivo* practice.

However, there are reports that show ^{31}P NMR spectra of bone recorded during *in vivo* studies. For example, Wu et al. (2011) presented a spectrum of bone mineral from a human wrist (Fig. 8a from that article). This spectrum reveals one complex line containing two evident components from AHSL and CAC, as in our study. Of course, the *in vivo* studies cannot be done with high-power decoupling (HPD). Nevertheless, the ^{31}P ssNMR signals acquired using the BD technique with and without HPD are quite similar (Wu et al., 2002). Moreover, we have found that HPD negligibly affects the T_1^P relaxation times of bone samples (see Supporting Material). Therefore, we suppose that the *in vivo* NMR spectroscopic studies of AHSL and CAC in human bone, based on our protocol, may be feasible.

Conclusions

In summary, for the first time the discrete morphological regions of nanoparticles of human bone mineral have been studied and their features associated with bone diseases.

We found that AHSL is fairly large as estimated from its phosphorus content. It accommodates up to 24% of phosphorus of bone mineral nanoparticles. The distribution of phosphorus between AHSL and CAC and the hydration levels of these nanoparticle compartments are dependent on the development of the bone diseases (OA, OPS/OPA). AHSL is more hydrated and disordered than CAC. This is because AHSL is amorphous, while CAC is crystalline. For both AHSL and CPC, there are positive correlations of T_1^P and negative correlations of *FWHM* with *B/A*. They indicate that with the increase of AHSL, both AHSL and CPC become less hydrated and more ordered. Between AHSL and CPC there is probably a transfer of water molecules, which affects CAC crystallinity. No correlations have been observed between the general macroscopic parameters of the skeletal system and the local molecular-level ssNMR parameters of the bone mineral.

In the trabecular bone of our specimens, OA predominates over OPS and elevates BMD. This is expressed by the negative correlation of T-score (lumbar spine) with *BV/TV* (femoral specimen). The ssNMR variables (*B/A*, T_1^P-CAC, T_1^P-AHSL, *FWHM*-CAC and *FWHM*-AHSL) can be represented by one principal component (*PC1*). *PC1* assists with patient classification and provides required insight into the bone mineral. Using the *PC1,* T-score and *BV/TV* variables, two main groups of patients have been identified: G1 and G2. G2 had both OA and OPS more developed than G1. Considering the *PC1* values, G2 had smaller AHSL than G1, more hydrated AHSL and CAC and both environments were less ordered. These changes in the bone mineral must have been caused by OA, because it is more influential than OPS in the trabecular bone tissue pertinent to the hip joint's functioning.

Overall, the ^{31}P ssNMR spectroscopy has proved to be a valuable method to selectively analyse the AHSL and CAC mineral compartments in whole bone.

Competing interests

The authors declare that they have no competing interests.

Acknowledgments

This study was supported by the Local Grant FW-23/N/2016 from the Medical University of Warsaw. The Laboratory of X-ray Densitometry of the Foundation "Center for the Development of Medicine" in Warsaw is acknowledged for the DEXA measurements.

Appendix A. Supplementary data

Supplementary data associated with this article can be found, in the online version, at http://dx.doi.org/10.1016/j.jab.2016.07.001.

References

Awonusi, A., Morris, M.D., Tecklenburg, M.M., 2007. Carbonate assignment and calibration in the Raman spectrum of apatite. Calcif. Tissue Int. 81, 46–52.
Bala, Y., Seeman, E., 2015. Bone's Material Constituents and their Contribution to Bone Strength in Health Disease, and Treatment. Calcif. Tissue Int. 97, 308–326.
Bertinetti, L., Tampieri, A., Landi, E., Ducati, C., Midgley, P.A., Coluccia, S., Martra, G., 2007. Surface structure, hydration and cationic sites of nanohydroxyapatite: UHR-TEM, IR and microgravimetric studies. J. Phys. Chem. C 111, 4027–4035.
Bartusik, D., Aebisher, D., 2015. Multinuclear magnetic resonance evaluation of tumor tissue. J. Appl. Biomed. 13, 69–78.
Boskey, A.L., 2013. Bone composition: relationship to bone fragility and antiosteoporotic drug effects. BoneKEy Reports 2 doi:http://dx.doi.org/10.1038/bonekey.2013.181 Article Number 447.
Boskey, A.L., Coleman, R., 2010. Aging and Bone. J. Dent. Res. 89, 1333–1348.
Cazalbou, S., Combes, C., Eichert, D., Rey, C., 2004. Adaptative physico-chemistry of bio-related calcium phosphates. J. Mater. Chem. 14, 2148–2153.
Cho, G., Wu, Y., Ackerman, J.L., 2003. Detection of Hydroxyl Ions in Bone Mineral by Solid-State NMR. Science 300, 1123–1127.
Combes, C., Cazalbou, S., Rey, C., 2016. Apatite Biominerals. Minerals 6, 34. doi: http://dx.doi.org/10.3390/min6020034.
Dawson, K.L., Farnan, I.E., Constantz, B.R., Young, S.V., 1991. Solid-state phosphorus-31 nuclear magnetic resonance differentiation of bone mineral and synthetic apatite used to fill bone defects. Inv. Radiol. 26, 946–950.
Duer, M.J., 2015. The contribution of solid-state NMR spectroscopy to understanding biomineralization: Atomic and molecular structure of bone. J. Magn. Reson. 253, 98–110.
Fantner, G.E., Rabinovych, O., Schitter, G., Thurner, P., Kindt, J.H., Finch, M.M., Weaver, J.C., et al., 2006. Hierarchical interconnections in the nano-composite material bone: Fibrillar cross-links resist fracture on several length scale. Compos. Sci. Technol. 66, 1205–1211.
Fratzl, P., Gupta, H.S., Paschalisb, E.P., Roschgerb, P., 2004. Structure and mechanical quality of the collagen–mineral nano-composite in bone. J. Mater. Chem. 14, 2115–2123.
Gaidash, A.A., Sintsa, L.N., Babenko, O.A., Lugovskoy, A.A., 2011. Nanoporous Structure of BoneMatrix at Osteoporosis from Data of Atomic Force Microscopy and IR Spectroscopy. J. Osteoporos. 1–7. doi:http://dx.doi.org/10.4061/2011/162041 Article ID 162041.
Glowacki, J., Hurwitz, S., Thornhill, T.S., Kelly, M., LeBoff, M.S., 2003. Osteoporosis and Vitamin-D Deficiency Among Postmenopausal Women with Ostheorthritis Undergoing Total Hip Arthroplasty. J. Bone Joint Surg. 85, 2371–2377.
Granke, M., Does, M.D., Nyman, J.S., 2015. The Role of Water Compartments in the Material Properties of Cortical Bone. Calcif. Tissue Int. 97, 292–307.
Gul-E-Noor, F., Singh, C., Papaioannou, A., Sinha, N., Boutis, G.S., 2015. Behavior of Water in Collagen and Hydroxyapatite Sites of Cortical Bone: Fracture, Mechanical Wear, and Load Bearing Studies. J. Phys. Chem. C 119, 21528–21537.
Hannemann, A., Friedrich, N., Spielhagen, C., Rettig, R., Ittermann, T., Nauck1, M., Wallaschofski, H., 2013. Reference intervals for serum osteocalcin concentrations in adult men and women from the study of health in Pomerania. BMC Endocrine Disorders 13, 11.
Im, G.-I., Kim, M.-K., 2014. The relationship between osteoarthritis and osteoporosis. J. Bone Miner. Metab. 32, 101–109.
Jäger, C., Welzel, T., Meyer-Zaika, W., Epple, M., 2006. A solid-state NMR investigation of the structure of nanocrystalline hydroxyapatite. Magn. Reson. Chem. 44, 573–580.
Jiang, L.-S., Zhang, Z.-M., Jiang, S.-D., Chen, W.-H., Da, L.-Y., 2008. Differential Bone Metabolism Between Postmenopausal Women With Osteoarthritis and Osteoporosis. J. Bone Miner. Res. 23, 475–483.
Kaflak, A., Kolodziejski, W., 2007. Phosphorus-31 spin-lattice NMR relaxation in bone apatite and its mineral standards. Solid State NMR 31, 174–183.
Kaflak, A., Kolodziejski, W., 2008. Kinetics of ^{1}H → ^{31}P NMR cross-polarization in bone apatite and its mineral standards. Magn. Reson. Chem. 46, 335–341.
Kaflak-Hachulska, A., Samoson, A., Kołodziejski, W., 2003. ^{1}H MAS and ^{1}H → ^{31}P CP/MAS NMR study of human bone mineral. Calcif. Tissue. Int. 73, 476–486.
Kolodziejski, W., 2005. Solid-state NMR of bone. Top Curr. Chem. 246, 235–270.
LeGeros, R.Z., 1991. Calcium phosphates in oral biology and medicine. In: Myers, H. M. (Ed.), Monographs in Oral Science 15. Karger, Basel.
Li, B., Aspden, R.M., 1997. Composition and mechanical properties of cancellous bone from the femoral head of patients with osteoporosis or osteoarthritis. J. Bone Miner. Res. 12, 641–651.
Maltsev, S., Duer, M.J., Murray, R.C., Jaeger, C., 2007. A solid-state NMR comparison of the mineral structure in bone from diseased joints in the horse. J. Mater. Sci. 42, 8804–8810.
McElderry, J.-D.P., Zhu, P., Mroue, K.H., Xu, J., Pavan, B., Fang, M., Zhao, G., McNerny, E., Kohn, D.H., Franceschi, R.T., Banaszak Holl, M.M., Tecklenburg, M.M.J., Ramamoorthy, A., Morris, M.D., 2013. Crystallinity and compositional changes in carbonated apatites: Evidence from ^{31}P solid-state NMR, Raman, and AFM analysis. J. Solid State Chem. 206, 192–198.
Michelsen, J., Wallaschofski, H., Friedrich, N., Spielhagen, C., Rettig, R., Ittermannc, T., Nauck, M., Hannemann, A., 2013. Reference intervals for serum concentrations of three bone turnover markers for men and women. Bone 57, 399–404.
Mroue, K.H., MacKinnon, N., Xu, J., Zhu, P., McNerny, E., Kohn, D.H., Morris, M.D., Ramamoorthy, A., 2012. High-Resolution Structural Insights into Bone: A Solid-State NMR Relaxation Study Utilizing Paramagnetic Doping. J. Phys. Chem. B 116, 11656–11661.
Mroue, K.H., Nishiyama, Y., Pandey, M.K., Gong, B., McNerny, E., Kohn, D.H., Morris, M.D., Ramamoorthy, A., 2015. Proton-Detected Solid-State NMR Spectroscopy of Bone with Ultrafast Magic Angle Spinning. Sci. Rep. 5, 11991. doi:http://dx.doi.org/10.1038/srep11991.
Mroue, K.H., Zhang, R., Zhu, P., McNerny, E., Kohn, D.H., Morris, M.D., Ramamoorthy, A., 2014. Acceleration of natural-abundance solid-state MAS NMR measurements on bone by paramagnetic relaxation from gadolinium-DTPA. J. Magn. Reson. 244, 90–97.
Nikel, O., Laurencin, D., Bonhomme, C., Sroga, G.E., Besdo, S., Lorenz, A., Vashishth, D., 2012. Solid state NMR investigation of intact human bone quality: balancing issues and insight into the structure at the organic-mineral interface. J. Phys. Chem. C Nanomater. Interfaces 116, 6320–6331.

Nyman, J.S., Ni, Q., Nicolella, D.P., Wang, X., 2008. Measurments of mobile and bound water by nuclear magnetic resonance correlate with mechanical properties of bone. Bone 42, 193–199.
Pajchel, L., Kolodziejski, W., 2013. Solid-state MAS NMR, TEM, and TGA studies of structural hydroxyl groups and water in nanocrystalline apatites prepared by dry milling. J. Nanopart. Res. 15, 1868–1882.
Pajchel, L., Kowalska, V., Smolen, D., Kedzierska, A., Pietrzykowska, E., Lojkowski, W., Kolodziejski, W., 2013. Comprehensive structural studies of ultra-fine nanocrystalline calcium hydroxyapatite using MAS NMR and FT-IR spectroscopic methods. Mater. Res. Bull. 48, 4818–4825.
Pasteris, J.D., Yoder, C.H., Wopenka, B., 2014. Molecular water in nominally unhydrated carbonated hydroxylapatite: The key to a better understanding of bone mineral. Am. Mineral. 99, 16–27.
Pett, M.A., Lackey, N.R., Sullivan, J.J., 2003. Making Sense of Factor Analysis. The Use of a Factor Analysis for Instrument Development in Health Care Research. SAGE Publications, London, UK.
Rai, R.K., Barbhuyan, T., Singh, C., Mittal, M., Khan, M.P., Sinha, N., Chattopadhyay, N., 2013. Total water, phosphorus relaxation and inter-atomic organic to inorganic interface are new determinants of trabecular bone integrity. PLoS One 8, e83478. doi:http://dx.doi.org/10.1371/journal.pone.0083478.
Rai, R.K., Sinha, N., 2011. Dehydration-Induced Structural Changes in the Collagen-Hydroxyapatite Interface in Bone by High-Resolution Solid-State NMR Spectroscopy. J. Phys. Chem. C 115, 14219–14227.
Rai, R.K., Singh, C., Sinha, N., 2015. Predominant Role of Water in Native Collagen Assembly inside the Bone Matrix. J. Phys. Chem. B 119, 201–211.
Rey, C., Combes, C., Drouet, C., Glimcher, M.J., 2009. Bone mineral-update on chemical composition and structure. Osteoporos. Int. 20, 1013–1021.
Reznikov, N., Shahar, R., Weiner, S., 2014. Bone hierarchical structure in three dimensions. Acta Biomater. 10, 3815–3826.
Primer on the Metabolic Bone Diseases and Disorders of Mineral Metabolism, In: Rosen, C.J., Bouillon, R., Compston, J.E., Rosen, V. (Eds.), 8th Ed. Wiley-Blackwell, Ames Iowa, USA.
The Aging Skeleton. In: Rosen, C.J., Glowacki, J., Bilezikian, J.P. (Eds.), Academic Press, San Diego, CA, USA.
Sakhno, Y., Bertinetti, L., Iafisco, M., Tampieri, A., Roveri, N., Martra, G., 2010. Surface hydration and cationic sites of nanohydroxyapatites with amorphous or crystalline surfaces: A comparative study. J. Phys. Chem. C 114, 16640–16648.
Samuel, J., Sinha, D., Zhao, J.C.-G., Wang, X., 2014. Water residing in small ultrastructural spaces plays a critical role in the mechanical behavior of bone. Bone 59, 199–206.
Seifert, A.C., Li, C., Rajapakse, C.S., Bashoor-Zadeh, M., Bhagat, Y.A., Wright, A.C., Zemel, B.S., Zavaliangos, A., Wehrli, F.W., 2014. Bone mineral ^{31}P and matrix-bound water densities measured by solid-state ^{31}P and ^{1}H MRI. NMR Biomed 27, 739–748.
Stock, R.S., 2015. The Mineral-Collagen Interface in Bone. Calcif. Tissue Int. 97, 262–280.
Sun, S.-S., Ma, H.-L., Liu, C.-L., Huang, C.-H., Cheng, C.-K., Wei, H.-W., 2008. Difference in femoral head and neck material properties between osteoarthritis and osteoporosis. Clin. Biomech. 23, S39–S47.
Techawiboonwong, A., Song, H.K., Leonard, M.B., Wehrli, F.W., 2008. Cortical bone water: In vivo quantification with ultrashort Echo-Time MR Imaging. Radiology 248, 824–833.
Timmins, P.A., Wall, J.C., 1977. Bone water. Calcif. Tissue Res. 23, 1–5.
Wang, Y., Euw, S.V., Fernandes, F.M., Cassaignon, S., Selmane, M., Laurent, G., Pehau-Arnaudet, G., Coelho, C., Bonhomme-Coury, L., Giraud-Guille, M.-M., Babonneau, F., Azaïs, T., Nassif, N., 2013. Water-mediated structuring of bone apatite. Nat. Mater. 12, 1144–1153.
Wehrli, F.W., Fernandez-Seara, M.A., 2005. Nuclear magnetic resonance studies of bone water. Ann. Biomed. Eng. 33, 79–86.
Wilson, E.E., Awonusi, A., Morris, M.D., Kohn, D.H., Tecklenburg, M.M.J., Beck, L.W., 2005. Highly ordered interstitial water observed in bone by NMR. J. Bone Miner. Res. 20, 625–634.
Wilson, E.E., Awonusi, A., Morris, M.D., Kohn, D.H., Tecklenburg, M.M.J., Beck, L.W., 2006. Three structural roles for water in bone observed by solid-state NMR. Biophys. J. 90, 3722–3731.
Wu, Y., Ackerman, J.L., Kim, H.-M., Rey, C., Barroug, A., Glimchel, M.J., 2002. Nuclear magnetic resonance spin-spin relaxation of the crystals of bone, dental enamel, and synthetic hydroxyapatites. J. Bone Miner. Res. 17, 472–480.
Wu, Y., Reese, T.G., Cao, H., Hrovat, M.I., Toddes, S.P., Lemdiasov, R.A., Ackerman, J.L., 2011. Bone Mineral Imaged In Vivo by ^{31}P Solid State MRI of Human Wrists. J. Magn. Reson. Imaging 34, 623–633.
Xu, Z., Yang, Y., Zhao, W., Wang, Z., Landis, W.J., Cui, Q., Sahai, N., 2015. Molecular mechanisms for intrafibrillar collagen mineralization in skeletal tissues. Biomaterials 39, 59–66.
Xu, J., Zhu, P., Morris, M.D., Ramamoorthy, A., 2011. Solid-state NMR spectroscopy provides atomic-level insights into the dehydration of cartilage. J. Phys. Chem. B 115, 9948–9954.
Zhang, Z.M., Jiang, L.S., Jiang, S.D., Dai, L.Y., 2009. Differential articular calcified cartilage and subchondral bone in postmenopausal women with osteoarthritis and osteoporosis: two-dimensional analysis. Joint Bone Spine 76, 674–679.
Zhao, N.,, 2009. The Minimum Sample Size in Factor Analysis. Available from: http://www.encorewiki.org/display/~nzhao/The Minimum Sample Size in Factor Analysis (accessed 29.03.16.).
Zhu, P., Xu, J., Sahar, N., Morris, M.D., Kohn, D.H., Ramamoorthy, A., 2009. Time-Resolved Dehydration-Induced Structural Changes in an Intact Bovine Cortical Bone Revealed by Solid-State NMR Spectroscopy. J. Am. Chem. Soc. 131, 17064–17065.